Comparative Study of Nanocomposites of Polyolefin Compatibilizers Containing Kaolinite and Montmorillonite Organoclays

Maria Pilar Villanueva,[1] Luis Cabedo,[1] José Maria Lagarón,[2] Enrique Giménez[1]

[1]*Area of Materials, Department of Industrial Systems Engineering and Design, University Jaume I, Campus Riu Sec, Castellón 12071, Spain*
[2]*Novel Materials and Nanotechnology Lab., Institute of Agrochemistry and Food Technology (IATA-CSIC), Apdo. Correos 73, Burjassot, Valencia 46100, Spain*

Received 8 October 2008; accepted 18 February 2009
DOI 10.1002/app.30278
Published online 7 October 2009 in Wiley InterScience (www.interscience.wiley.com).

ABSTRACT: This work studied the morphology and physical properties of nanocomposites of different ethylene copolymers and functionalized polyethylenes with two different types of organoclays, to assess the potential application of these fillers as reinforcing components in the design of polyethylene and other polyolefinic based nanocomposites with enhanced properties. A polyethylene-grafted-maleic anhydride (PEMA), a poly(ethylene-co-acrylic acid), a poly(ethylene-co-vinyl acetate), and an ionomer of poly(ethylene-co-methacrylic acid) containing a small fraction of polyamide 6 were used to prepare nanocomposites by melt compounding in internal mixer. Two different types of commercial clays were used to obtain nanocomposites with the same organoclay content (5 wt %), i.e., an organomodified montmorillonite and an organomodified kaolinite. The morphology was evaluated by wide angle X-ray scattering, scanning electron microscopy, transmission electron microscopy, and optical microscopy. The thermal, mechanical and barrier properties were evaluated by differential scanning calorimetry and thermogravimetric analysis, tensile tests and oxygen transmission rate experiments, respectively. From the results, it was seen that PEMA and the ionomer are the best polymer matrices to disperse both organoclays under the conditions applied. Kaolinite and montmorillonite appeared to be dispersed in the nanorange, however, higher aspect ratio was observed for montmorillonite. The best improvements in thermal degradation and in mechanical reinforcement were shown for organomodified kaolinite nanocomposites. But the best improvements in thermo-oxidative degradation and in oxygen barrier were seen for the nanocomposites with organomodified montmorillonite. © 2009 Wiley Periodicals, Inc. J Appl Polym Sci 115: 1325–1335, 2010

Key words: polyolefin compatibilizers; nanocomposites; organoclays; kaolinite; montmorillonite

INTRODUCTION

Polyethylene (PE) is one of the most consumed polyolefins in the world. The use of this polymer is highly extended because of its extraordinary versatility in terms of properties, applications, and low cost. In the last years, its use in packaging applications, where mechanical, barrier properties, and transparency are important, has increased.[1] Polyolefins offer a good barrier to humidity but are highly permeable to oxygen. As a result, many of the polymer properties (mechanical, thermal, and barrier properties) have been challenged by incorporation of fillers. Conventional fillers such as silica, glass fiber, talc, wood flour, cellulose, etc, have been used to form traditional microcomposites with enhanced properties.[2–7] But in the last decade, a great interest in polymer-layered silicate nanocomposites has emerged. With the incorporation of layered nanoclays as fillers, having high aspect ratio (length/thickness) and thicknes in the nanometer range, it has been possible to improve mechanical, thermal and barrier properties at lower loadings (usually less than 10%) than for conventional fillers. This is possible due to the nanoscale reinforcement and the more tortuous diffusion path caused by the dispersion of the high aspect ratio layers and/or thin clay agglomerates so-called tactoids. These improved properties may be due to the synergic effects of nanoscaled structure and the resulting enlarged interaction of the layered inorganic materials with the polymer molecules.[8,9]

Because of the non-polar backbone of polyethylene and polyolefins in general, there is an inherent poor adhesion between the polar natural clay and the polymer when mixed by conventional melt-mixing techniques. Nevertheless, researchers have attempted to enhance the interaction between clay and polyethylene by modifying clay surface with alkylammonium

Correspondence to: E. Giménez (enrique.gimenez@esid.uji.es).

salts, among others, and using compatibilizers in the mixing process.[10] Aggregated/intercalated structures are common morphologies when alkylammonium treated montmorillonites are melt blended with polyethylene.[11] Better dispersion is achieved using polyethylene-grafted-maleic anhydride as compatibilizer, which can enhance the intercalation of the polymer chains within the silicate gallery.[12–18] The addition of a compatibilizer intends to reduce the interfacial energy between the polymer and the filler, resulting in better adhesion and finer dispersion of the layered silicates. However, the improvements achieved in the final nanocomposite depend on many factors, such as the type and content of polar groups inserted in the polymer backbone, the amount of the overall compatibilizer added, the method used for the preparation, the processing parameters and obviously the type of filler and its fraction in the final compound. It has been shown that the extent of intercalation and exfoliation of the clay platelets by the polymer chains greatly determines the degree of enhancement of mechanical, thermal and barrier properties.[19]

To date, the main efforts in polyethylene nanocomposites have been focused on the development of polymer-clay nanocomposites with montmorillonitic clays. In this work, our efforts are centered on the comparative development of inorganic-organic hybrid nanocomposites with two different commercial clays: a kaolinite-based organoclay and a montmorillonite-based organoclay. Although there are some reported studies about the effect of kaolinite in other polymers such as nylon 6, polyethylene oxide, poly(vinyl pyrrolidone), polyhydroxybutyrate, ethylene-vinyl-alcohol, poly(lactic acid), and polyethylene glycol,[20–25] the influence in polyolefinic matrices is still not reported. Kaolinite ($Al_2Si_2O_5(OH)_4$) is a 1 : 1 phyllosilicate containing a gibbsite octahedral layer and a silicon oxide tetrahedral sheet. This asymmetric structure allows the formation of hydrogen bonds between consecutive layers, providing large cohesive energy. As a consequence of the high layer-to-layer interactions, the intercalation of the polymer chains between the kaolinite platelets is greatly impeded, thus rendering a chemical treatment of the mineral surface.[20] Kaolinite has limited exchangeable cations in its interlayer region, thus its organic modification does not necessarily imply cationic exchange reactions. However, organic molecules (dimethylsulfoxide, methylformamide, benzamide, polyvinylpyrrolindone, etc) can be adsorbed in the kaolinitic surface increasing the basal spacing as it has been reported is several previous articles.[26–34] Generally, kaolinite is first modified by a precursor (i.e., dimethylsulfoxide, N-methyl formamide) in order to avoid the formation of hydrogen bonds. Once the precursor molecules have been inserted in the intergallery region, larger molecules (i.e., alkylammonium salts, polyethylene glycol, carboxy-methylcellulose, aminoacids) can be inserted to improve the affinity with polymeric chains. In this second step, the precursor is mainly substituted from other molecules and the basal spacing is incremented.[35–37] Despite the inherent difficulty of kaolinite to be organomodified, this clay also has a very high aspect ratio and previous works show more favorable barrier properties and polymer stability than using montmorillonite.[23] Montmorillonite is a 2 : 1 phyllosilicate. The crystalline structure of this material consists of an octahedral aluminium hydroxide sheet sandwiched in between two silicate tetrahedral layers. Stacking of the layers leads to a regular van der Waals gap between the layers called the interlayer gallery. An isomorphic substitution of the aluminium or silicon within the layers generates negative charges that are counterbalanced by hydrated cations adsorbed on the interlayer space. These cations can be exchanged with cationic surfactants to modify the surface of the montmorillonite.[8]

This work reports for the first time about the interactions between various ethylene copolymers or functionalized polyethylenes and two different organoclay systems (based on montmorillonite and kaolinite) to investigate their suitability as potential compatibilizers in the development of PE and other polyolefin nanocomposites. Some preliminary results on morphological and physical properties of these systems were previously presented.[38] Nevertheless, the current article presents a full description of the nanocomposites with a more extended morphological characterization [wide angle X-ray scattering (WAXS), optical microscopy, scanning electron microscopy (SEM), transmission electron microscopy (TEM)], oxygen barrier properties and a more detailed explanation of mechanical and thermal properties.

EXPERIMENTAL

Materials

The polyethylene grafted with maleic anhydride (FUSABOND® E MB226DE), so-called throughout the article PEMA, the copolymer of ethylene and acrylic acid (ELVALOY® 3717 AC), so-called throughout the article as PEAA and the ionomer containing a small fraction of polyamide 6 (Surlyn® AM-7928) so-called throughout the article as Ionomer were supplied by DuPont Iberica S.L. (Barcelona). Ethylene vinyl acetate copolymer (EVATANE® 1020 VN3) so-called throughout the article EVA was provided by AtoFina Spain (Elf Atochem). The density, the melt flow index (MFI), the melt temperature (T_m), and the level of polar groups

TABLE I
Characteristics of the Polymeric Matrices Used in this study: Content of Polar Groups, Density, Melting Temperature (T_m), and Melt Flow Index (MFI)

Polymer matrix	Polar groups	Density (g/cm^3)	T_m (°C)	MFI (g/10 min)
PEMA	0.9% MA	0.93	120	1.5 (190°C, 2.16 Kg)
PEAA	17% AA	0.924	96	7 (190°C, 2.16 Kg)
Ionomer	Not supplied	0.98	85	10 (230°C, 2.16 Kg)
EVA	9% VA	0.929	98	3 (190°C, 2.16 Kg)

in the different functionalized matrices are summarized in Table I.

Cloisite® 20A, a montmorillonite (so-called MMT) grade chemically modified with dimethyl, dihydrogenatedtallow ~65% C18/~30% C16/~5% C14, quaternary ammonium salt, was purchased from Southern Clay Products Incorporation, US. Calcination losses by TGA were of ca. 38% for this organoclay.

A proprietary food contact legislation complying phyllosilicate experimental grade (NanoBioter® D14) based on a patent pending organomodified kaolinite (so-called K) was supplied by NanoBioMatters S.L., Spain. No further details of clay preparation and modification were disclosed by the manufacturer. Calcination losses by TGA were of ca. 20% for this organoclay.

Preparation of the nanocomposites

Before mixing, compatibilizers and organoclays were dried between 60 and 80°C, under vacuum for 24 h, to remove moisture. Nanocomposite samples having 5 wt % organoclay loadings were obtained by melt mixing the two components in an internal mixer (Haake Polylab) at a temperature of 140°C and a rotor speed of 100 rpm for three minutes to avoid excessive thermal exposure of the organoclays. Sheets and films were prepared by compression moulding from grinded material at 150°C. These hot-pressed sheets and films were quenched in water and were used to carry out the characterization of the samples. The organic fraction of each commercial organoclay was determined from thermogravimetric tests, to calculate the inorganic percentage of clay in the compounded nanocomposites. From the results, a 3.1% and 4% of inorganic content was present for montmorillonite and kaolinite, respectively.

Characterization techniques

WAXS were performed using a Bruker AXS D4 Endeavour diffractometer. Radial scans of intensity versus scattering angle (2θ) were recorded at room temperature in the range 2-30° (step size = 0.02° (2θ), scanning rate = 8 s/step) with identical setting of the instrument by using filtered CuK_α radiation ($\lambda = 1.54$Å), an operating voltage of 40kV, and a filament current of 30 mA. To calculate the clays d-spacing, Bragg's law ($\lambda = 2d \sin\theta$) was applied.

Optical micrographs were obtained by an optical microscope Leica (model DM-RME). Observations were made in the transmission mode on nanocomposite films of approximately 100 μm thickness prepared by melt pressing. The micrographs represented here were obtained with a magnification of 200x.

SEM was also used to better resolve and asses the dispersion of clay in the nanocomposites. SEM images were taken from cryofractured samples using a Leo SEM (model 440i).

The dispersion of the clay layers was also observed by TEM. Nanocomposite samples were inserted in an epoxy resin and were cut in ultrafine sections with an ultramicrotome at room temperature. Observations were made using a Jeol 1010 (100 kV).

Tensile properties were measured by an universal testing machine (Instron 4469) at a crosshead speed of 10 mm/min and room temperature. Tests were made according to ASTM D638 using films of approximately 200 μm thickness prepared by compression moulding.

Differential scanning calorimetry (DSC) experiments were recorded using a Perkin-Elmer DSC7 calorimeter on 8-10 mg of material using argon as the purging gas. The calibration of the DSC was performed with a standard sample of indium. The thermal program applied for all samples, except the ionomer, was a first heating step between 50°C and 180°C at 10°C/min followed by an isotherm at 180°C during 2 min, a cooling step between 180°C and 50°C at 10°/min, and a second heating step from 50°C to 180°C at 10°C/min. The ionomer specimens were heated until 200°C due to the presence of a small fraction of the polymer melting at ca. 194°C. Melting temperatures (T_m) and melting enthalpies (ΔH_m, normalized for the polymer content in the nanocomposites) were calculated from the second heating step. Crystallization temperatures (T_c) and crystallization enthalpies (ΔH_c, normalized for the polymer content in the nanocomposites) were also calculated in the cooling step to see the effect of clay in the crystallization process.

Themogravimetric analyses (TGA) were developed in a TGA/SDTA 851e Metter-Toledo at a heating scan of 10°C/min, in argon and air atmosphere.

Oxygen permeability of the samples was measured with an Oxtran permeability apparatus (OXTRAN 100A equipped with a DL-200 Data Logger, Mocon, Minneapolis, MN) at 25°C and 80% relative humidity provided by the incorporated gas bubblers and monitored by a hygrometer. Before testing the samples were kept in a desiccator at 80% RH.

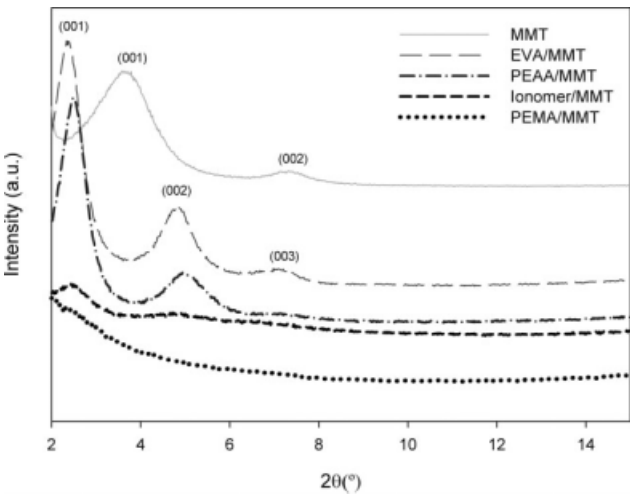

Figure 1 WAXS patterns of oganomontmorillonite-based nanocomposites.

RESULTS AND DISCUSSION

Nanocomposites morphology

The combination of WAXS and TEM has been extensively used in the literature to characterize the morphology of polymer-clay nanocomposites. In this study, both techniques were used to extract useful information in combination with SEM and optical microscopy observations.

The morphological analysis by WAXS of the montmorillonite nanocomposites shows that intercalated and/or exfoliated structures are generally obtained with all based polyolefinic compatibilizers. Thus, the WAXS diffraction patterns reveal that MMT (Fig. 1) presents a strong diffraction peak at 3.6°(2θ) which corresponds to the fraction of modified clay with an interlayer distance of 2.4 nm ($d_{(001)}$ calculated by Bragg's equation), and another peak at 7.2° (2θ) which corresponds most likely to the second-order diffraction peak.[14,39] In PEAA/MMT and EVA/MMT there is an increase in the interlayer spacing, as derived from the displacement of the (001) peak towards lower angles. According to Bragg's law, the intergallery spacing for PEAA/MMT is 3.5 nm and 3.6 nm for EVA/MMT. There are also two minor peaks, that are observed at 5°(2θ) and 7.5°(2θ) for the PEAA/MMT system and at 4.8°(2θ) and 7.2°(2θ) for the EVA/MMT system, which can be associated with the second and third-order diffraction harmonic peaks, respectively. The latter reflections are observed in these two matrices and not in the other two compatibilizer matrices used, ought to a more regular stacking of the clay dispersed within these particular polymers. Basal spacing of Ionomer/MMT is also 3.5 nm but the diffractogram shows a less intense and wider (001) peak. Moreover, the second and third-order peaks are practically not seen for this composite. All the above observations could in principle suggest a good dispersion and a lower tactoid size for the MMT in the ionomeric matrix compared with PEAA and EVA nanocomposites.

The PEMA system seems to intercalate easier into the MMT layers (Fig. 1). Thus, in the PEMA/MMT system, the characteristic basal peak of the clay disappear, strongly suggesting a high level of exfoliation for the clay layers within the polymer matrix.[40] Nevertheless, this high dispersion and exfoliation is not truly observable at the microscale, since some small clay aggregates can still be observed by optical microscopy (see later).

Figure 2 shows the diffraction patterns of the nanocomposites with organomodified kaolinite. As it can be seen, *K* presents a basal peak at ca.7.9°(2θ) which corresponds to the modified clay with a d-spacing of 1.11 nm. A residual peak at 12.4°(2θ) can also be seen that is attributed to a fraction of unmodified kaolinite ($d = 0.72$ nm). This means that the clay is not completely modified, and a residual fraction remains at the natural stacking distance. Kaolinite, as well as nanocomposites containing this clay, present another diffraction peak at 9°(2θ) which can be ascribed to the (003) peak of illite, i.e., a residual mineral component of the kaolinite (see the pattern of the unmodified kaolinite). In the nanocomposites, the modified peak is no longer observed and it can perhaps be only discerned in the pattern of the EVA/K system. This could in turn suggest that a high level of intercalation is taken place in general for these systems; however, a careful look at the diffraction patterns indicates that the basal peak for the natural kaolinite can be more clearly observed than in the organomodified kaolinite clay patterns (see the basal peak intensity ratio illite/kaolinite). The somewhat rising presence of the natural kaolinite peak in the melt compounded composites

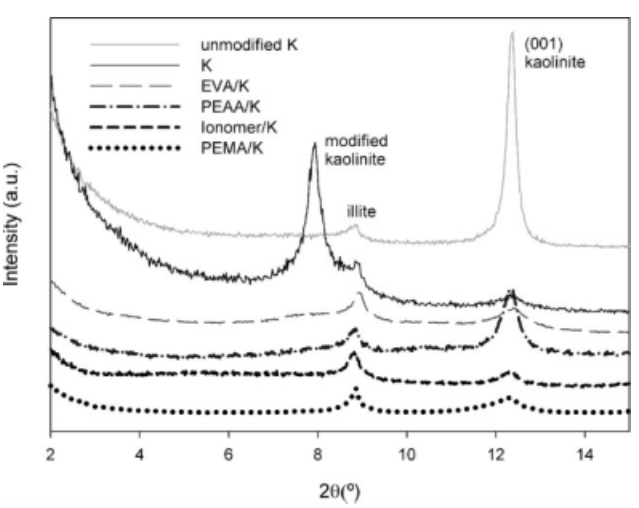

Figure 2 WAXS patterns of organokaolinite-based nanocomposites.

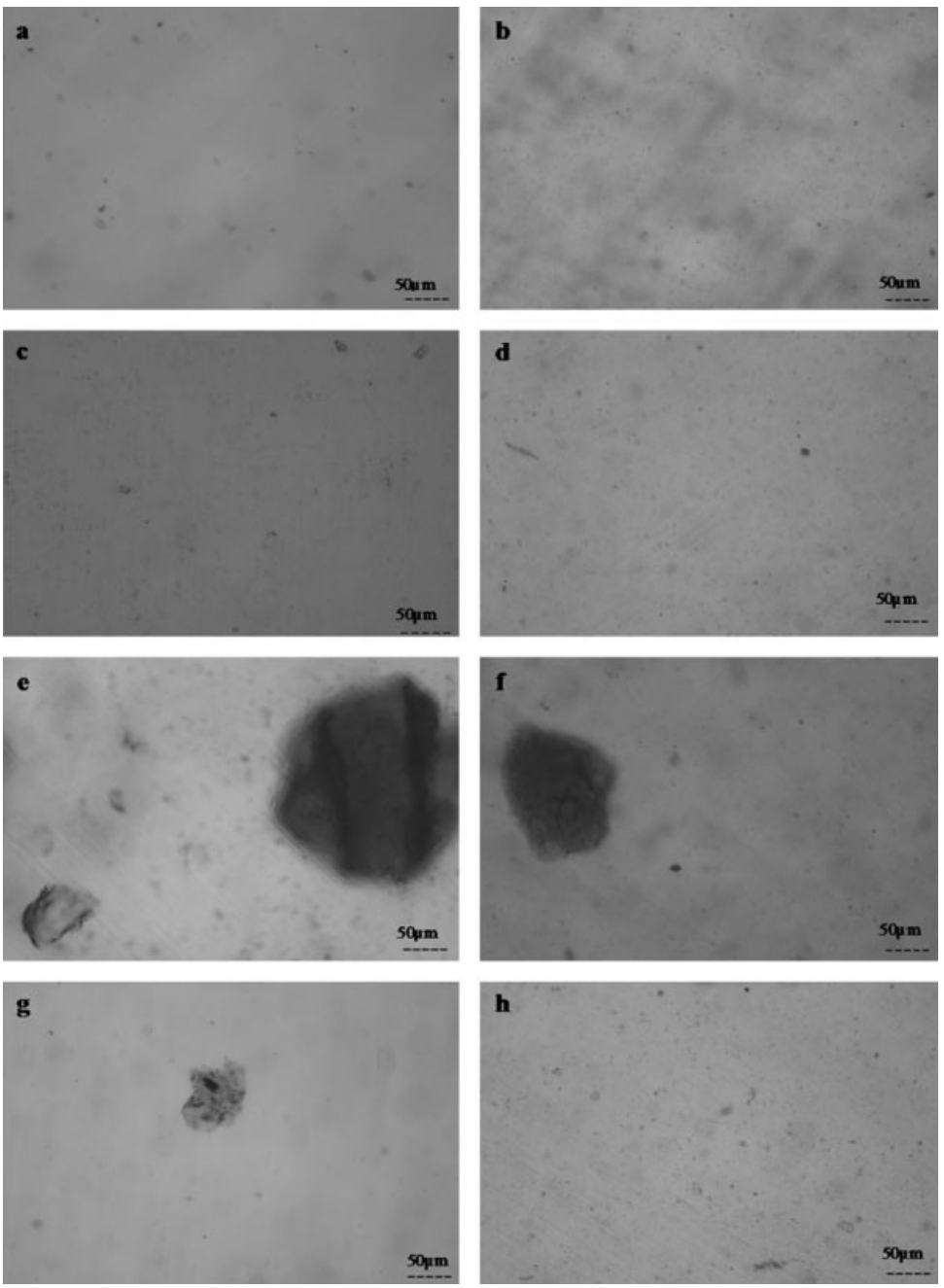

Figure 3 Micrographs obtained by optical microscopy: (a) PEMA/MMT, (b) PEMA/K, (c) Ionomer/MMT, (d) Ionomer/K, (e) PEAA/MMT, (f) PEAA/K, (g) EVA/MMT, (h) EVA/K; the scale of each micrograph is 50 µm.

does thus suggest that, to some extent, the modification of the clay is lost during compounding reverting some of the clay to its original stack distance in the nanocomposite. From past efforts, the clay fraction that is in the natural state and the fraction that is intercalated or exfoliated cannot be unambiguously determined. The same effect was previously reported in polyhydroxybutyrate-kaolinite nanocomposites.[23] In our systems, it seems that the PEMA/K, Ionomer/K, and EVA/K samples could present better dispersion and lower size of kaolinite aggregates as indicated by the lower and broader intensity of the kaolinite peak respect to the sample PEAA/K. The latter observations are corroborated by the size of clay aggregates observed by optical microcopy (see later).

Thin films of all samples were also observed by optical microscopy (Fig. 3) to characterize the morphology at the microscale. Apparently, both types of clays present good dispersion in the PEMA and ionomer matrices where small aggregates of only a few micrometers can be seen homogeneously dispersed in the polymer (Fig. 3a, 3b for PEMA and 3c, 3d for Ionomer). In the systems with PEAA [Fig. 3(e,f)] a really

bad dispersion can be seen for both types of clays (immiscible system). However, as previously reported by other authors,[41] ethylene-acrylic acid copolymers can be good matrices to disperse organoclays. In our case, the reason for the agglomeration of the clays could be the high content of acrylic acid groups (17%) that contain the particular copolymer used, perhaps making the polymer too polar for a good compatibilization with the organoclays. Samples based on the EVA copolymer were seen to have a good dispersion only when the clay used was kaolinite [Fig. 3(h)], however, there is a higher density and concentration of microaggregates compared to PEMA and ionomer nanocomposites. For the EVA/MMT nanocomposite, there is a bad dispersion of the clay as can be appreciated from the big aggregates [Fig. 3(g)].

SEM and TEM pictures (Fig. 4) were taken for the PEMA and ionomer samples due to the better

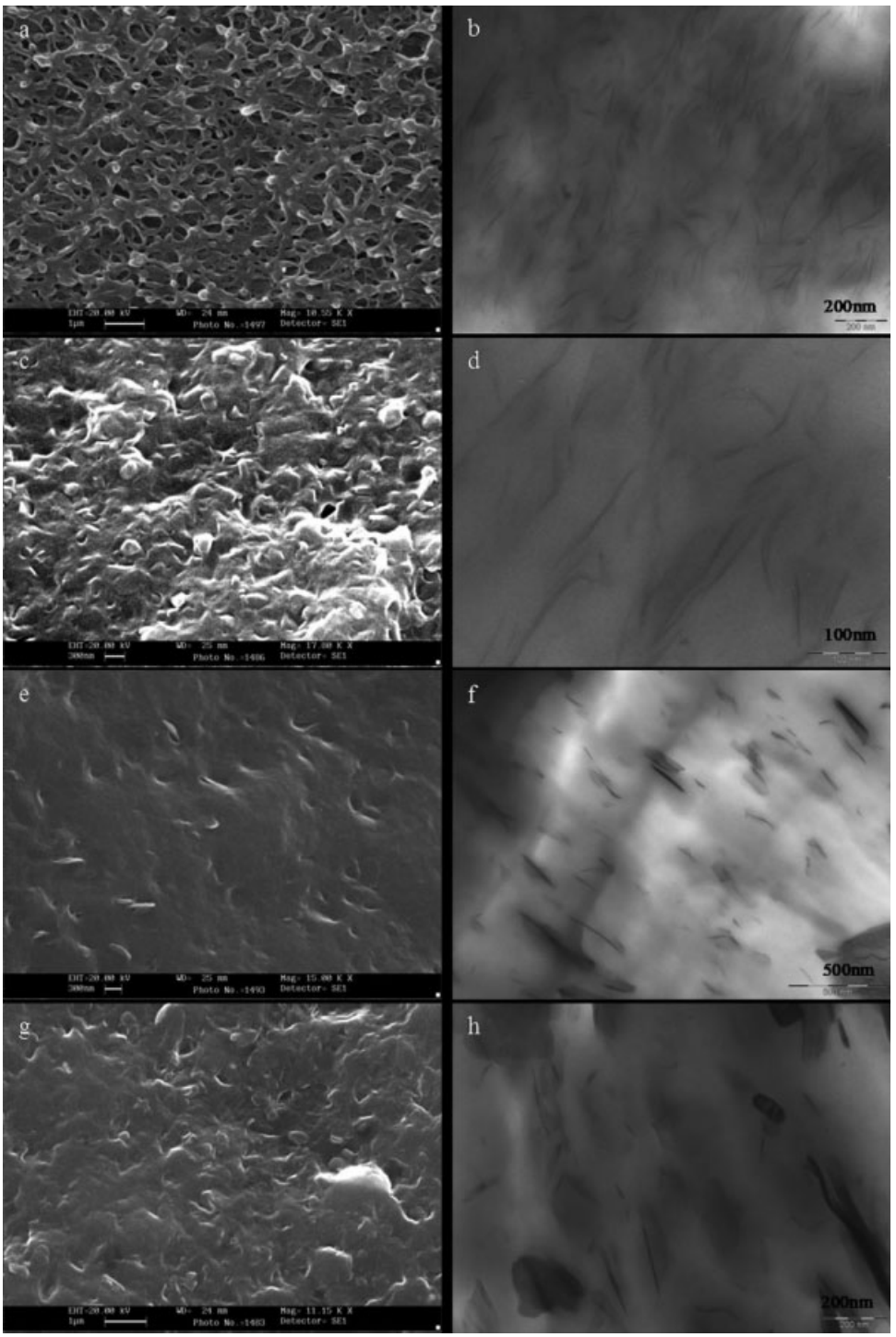

Figure 4 SEM and TEM pictures of (a,b) PEMA/MMT; (c,d) Ionomer/MMT; (e,f) PEMA/K; (g,h) Ionomer/K.

TABLE II
Aspect Ratios (L/W) Measured by TEM, Calculated by the Halpin-Tsai Mechanical Model and Determined by the Nielsen Permeability Model

System	L/W by TEM	L/W by Halpin-Tsai	L/W by Nielsen
PEMA/K	20–30	22	20
Ionomer/K	4–20	15	12
PEMA/MMT	30–60	22	60
Ionomer/MMT	20–50	10	35

results measured for these matrices by WAXS and optical microscopy. Figure 4(a) suggests a good adhesion between the MMT clay and the PEMA matrix (clay tactoids were detected under the polymer matrix), whereas the TEM image in Figure 4(b) shows the good dispersion and exfoliation of the clay. The dark lines represent individual sheets or tactoids of a few platelets (1–5 nm in thickness) of approximately 100 nm in length. Nevertheless, exfoliation is not complete as the optical microscope showed the presence of some bigger particles. Montmorillonite is also well adhered, dispersed and partially exfoliated in the ionomer matrix [Fig. 4(c,d)] despite the presence of some microaggregates observed by optical microscopy.

SEM and TEM pictures for the kaolinite-based nanocomposites indicate that this clay exhibits good adhesion with the PEMA and ionomer matrices and is intercalated or partially exfoliated, due to the favorable interactions produced between the polar groups of the polymers and the kaolinite surface [Fig. 4(e–h)]. The degree of exfoliation achieved for the PEMA/K sample is higher than for the Ionomer/K, however, aspect ratio was higher for the montmorillonite systems. The kaolinite tactoids are formed by a few platelets (10–20 nm in thickness). The aspect ratio of the samples as estimated from the TEM images is summarized in Table II.

From the above results, it seems that SEM, TEM, WAXS, and optical microscopy need to be combined to fully assess the morphology and dispersion of nanoclays at the nano and microscale.

Mechanical properties

Regarding the mechanical properties, all the nanocomposites show an improvement in stiffness (elastic modulus) compared with the unfilled polymer (Table III). According to the TEM observations, it is seen that montmorillonite is better dispersed into higher aspect ratio particles than is the kaolinite clay in the PEMA and ionomer matrices. However, larger increase in the modulus was observed for PEMA and ionomer when kaolinite was added contrarily to what could be expected. This can be attributed to the higher inorganic content in the organokaolinite but it could also be related to a different interfacial adhesion between these two clays and the polymer, more favorable for the kaolinite system in this case, and to the different tactoid size, being the lower aspect ratio of the kaolinite positive for a higher increment in the stiffness.

In montmorillonite nanocomposites, the addition to 5 wt % improved the stiffness of the PEMA matrix by an average of 47% and by 26% in the ionomer matrix. Similar or lower improvements were previously reported for montmorillonite nanocomposites based on PEMA,[18,42] while higher mechanical properties where achieved in ionomer nanocomposites prepared by twin screw extrusion.[43] However, kaolinite nanocomposites showed an improvement of 71% in the PEMA matrix and of 55% in the ionomer matrix. Maleated polyethylene based nanocomposites exhibited the highest elongation at break (>500%), the samples elongated to the maximum drawing limit of the machine without failure.

TABLE III
Mechanical and Thermal Properties of Nanocomposites: Elastic Modulus (E), Stress at Break (σ_b), Crystallization Temperature (T_c), Melting Temperature (T_m), Crystallization Enthalpy (ΔH_c), and Melting Enthalpy (ΔH_m)

Sample	E (MPa)	σ_b (MPa)		T_c (°C)			T_m (°C)			ΔH_c (J/g)			ΔH_m (J/g)	
PEMA	175 (±27)	[a]		99.3			119.7			−79.8			83.2	
PEMA/K	300 (±31)	[a]		103.3			120.4			−81.5			89.1	
PEMA/MMT	257 (±41)	[a]		102.9			120.0			−80.0			87.4	
Ionomer	254 (±13)	15.4 (±0.9)	63.6	—	92.4		194.4	−40.6		—	48.9			4.2
Ionomer/K	393 (±24)	17.6 (±0.2)	70.3	146.3	92.0		194.0	−46.9		−3.3	51.4			1.9
Ionomer/MMT	319 (±30)	16.8 (±1.0)	69.3	162.6	92.7		189.0	−46.3		−2.2	53.3			1.2
EVA	63 (±4)	≥11.1 (±0.5)[a]		77.9			97.0			−52.2			47.4	
EVA/K	73 (±5)	≥10.6 (±0.3)[a]		78.3			97.0			−50.6			47.9	
EVA/MMT	115 (±12)	8.6 (±0.5)		78.3			97.0			−53.0			47.3	
PEAA	40 (±2)	≥7.9 (±0.3)[a]		77.9			97.0			−37.4			32.8	
PEAA/K	47 (±2)	6.5 (±0.3)		79.6			98.0			−33.7			32.7	
PEAA/MMT	55 (±3)	5.9 (±0.8)		79.3			97.7			−35.6			32.6	

[a] These samples elongate until the maximum drawing limit of the machine without failure, at the test conditions used

However, ultimate stress is slightly increased in ionomer nanocomposites with regard to the unfilled ionomer.

Samples based on PEAA present a small increment in the elastic modulus; however, the addition of clay resulted in an immiscible system as was suggested by the poor dispersion of the clay. In this case, the reduction in the ultimate stress with respect to PEAA can be an indication of poor affinity between the components. It should be stated that the value of the neat PEAA corresponds to the tensile stress registered when the machine reached the maximum drawing limit, thus the unfilled PEAA does not break at the conditions used during the tensile tests, but nevertheless it should be above 7.9 MPa. Finally, the EVA matrix provided results which suggest that kaolinite is better dispersed at the microscale than montmorillonite (according to the optical micrographs), however, the improvement in stiffness is better for the case of the montmorillonite nanocomposites. Nevertheless, for this matrix it is worth noting that both EVA nanocomposites presents lower stress at break with regard to the unfilled EVA, possibly due to the weak affinity between the polymer and clay.

The obtained elastic modulus of PEMA and ionomer nanocomposites were fit to a mechanical model to explain the influence of the clay nature and hence, of the different modification methods generally used for montmorillonite and kaolinite clays. The modeling for elastic modulus proposed by Halpin-Tsai model [eq. (1)] and referred widely in the literature was used to predict the aspect ratio of layered silicate nanocomposites.[44-48]

$$Ec = Em\left[\frac{1+\zeta\eta\phi_f}{1-\eta\phi_f}\right] \quad (1)$$

$$\eta = \frac{Ef/Em-1}{Ef/Em+\zeta} \quad (2)$$

$$\zeta = 2(\mathrm{L/W}) \quad (3)$$

Where E_c is the elastic modulus of the composite, E_m is the elastic modulus of the matrix, φ_f is the inorganic volume fraction of clay, η is a geometric factor that is given by eq. (2) and that depends on the factor ζ, E_f is the elastic modulus of the filler and L/W is the aspect ratio of the dispersed clay particles. In this study, the volume fraction was calculated using the inorganic content of the organoclay and density values of 2.3 g/cm^3 and 2.6 g/cm^3 for K and MMT, respectively.[49] The micromechanical model was used to calculate the aspect ratio (L/W) of the samples (Table II). The model was applied in the systems PEMA/K, ionomer/MMT, and ionomer/K only for the clay content studied in this work, however, for the system PEMA/MMT (which presents the highest level of exfoliation) the aspect ratio was calculated from the results obtained for different clay contents (5, 10, 20 wt % of organomontmorillonite) (Fig. 5).

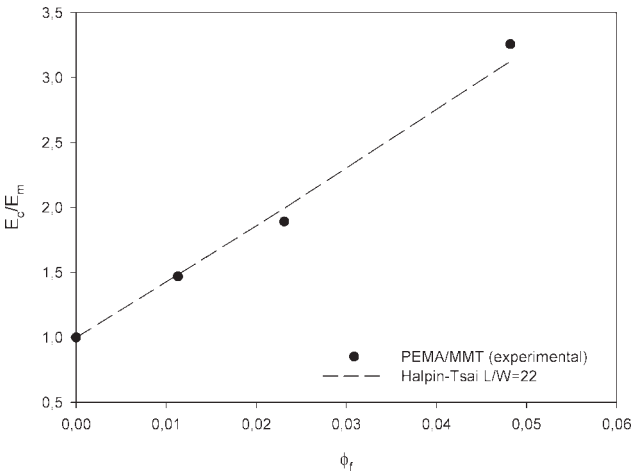

Figure 5 Relative elastic modulus (E_c/E_m) and theoretical curve resulted from application of Halpin Tsai model for the system PEMA/MMT.

The experimental values of E_c/E_m seem to fit for different aspect ratios depending on the type of clay and matrix. L/W values predicted by the Halpin-Tsai model are summarized in Table II, where it can be observed that theoretical aspect ratios predicted for kaolinite nanocomposites are in the range of the experimental values as estimated from the TEM pictures. However, the predicted values for montmorillonite nanocomposites are lower than the experimental data. It is important to stress that this model assumes full adhesion between clay particles and the matrix, considers only one direction in the orientation of clay particles and assumes a homogeneous distribution of the filler in the matrix. According to the results obtained for kaolinite nanocomposites, kaolinite may be better adhered to the PEMA and ionomer matrices. A higher adhesion between PEMA and ionomer matrices and kaolinite could be due to the different surface chemistry of this clay and the lower fraction of a polar organic modifier used.

Therefore, it is deduced that Halpin-Tsai model can only be used to predict the aspect ratio of the kaolinite nanocomposites and not for the montmorillonite compounds.

Thermal properties

To determine the effect of the clay filler in the crystallinity of the nanocomposites, the melting and crystallization points and the corresponding enthalpies were calculated by DSC (Table III). From the results, it is observed that in general there are no

TABLE IV
Degradation Temperatures Obtained From TGA Tests

Sample	T_{50} (°C) in argon	T_{50}(°C) in air	Sample	T_{50} (°C) in argon	T_{50}(°C) in air
PEMA	471.0	395.6	EVA	467.7	402.3
PEMA/MMT	457.2	426.0	EVA/MMT	452.2	430.3
PEMA/K	473.2	408.6	EVA/K	467.9	428.3
Ionomer	463.0	428.3	PEAA	454.6	363.0
Ionomer/MMT	464.9	445.3	PEAA/MMT	464.3	423.6
Ionomer/K	464.6	432.6	PEAA/K	466.9	402.0

significant changes in melting or crystallization of EVA and PEAA nanocomposites, whatever the clay nature.

The effect of the addition of clay to the maleated polyethylene (PEMA) or to the ionomer matrix seems more relevant in terms of impacting the DSC results. These nanocomposites show slightly higher crystallization temperatures and higher melting enthalpies with respect to the unfilled matrices. These results suggest that the addition of clay may have a nucleating role in these matrices. In the PEMA/K system, both T_c and enthalpies are slightly higher than for the samples with montmorillonite, as a consequence of the potentially higher interactions with the kaolinite clay. The nucleating effect of clay in polyethylene-grafted-maleic anhydride has been previously reported.[18] A different behavior is, however, observed in the crystallization process for the ionomer nanocomposites. With the addition of kaolinite or montmorillonite the ionomer presents two crystallization peaks, which are not detected in the neat polymer. The most intense peak corresponds to the crystallization of the ethylenic chains and the less intense peak possibly to the polyamide fraction existing in this material.

TGA analysis shows the effect of the mineral filler in the thermal degradation of the polymer matrix. From the results, the thermal stability under argon atmosphere is decreased when MMT is added to PEMA or EVA. This could be due to the specific modification of the montmorillonite clay with ammonium salts which by means of a Hoffman elimination process could lead to degradation of the polymer matrix.[50] As opposite to that an enhancement in thermal stability for the nanocomposites containing kaolinite was measured (Table IV).

The thermo-oxidative behaviour of the samples was also followed by TGA tests carried out using air as the purging gas. The nanocomposites present a remarkable delay in the thermo-oxidative degradation. Addition of clay is thought to cause a barrier effect to the oxygen diffusion into the polymer matrix and a barrier to the transport of volatile products coming out from the degradation of the sample.[51] The temperature at which a weight loss of 50% ($T_{0.5}$) occurs is higher for the montmorillonite nanocomposites (Table IV). This could be due to the higher barrier imposed by the montmorillonite layers, which seem to have higher aspect ratio (length/thickness) than the compounded kaolinite layers (according to TEM pictures).

Oxygen permeability

Oxygen transmission rate measurements were finally taken in PEMA and ionomer nanocomposites as they exhibit the best properties and morphology. The oxygen permeability measurements (Fig. 6) indicate that a relatively low decrease in permeability is seen for these nanocomposites with the clay loadings used. The best barrier performance is exerted by the PEMA/MMT specimens ($1.62.10^{-17}$ m^3m/m^2sPa), which show a permeability reduction of ca. 27.3% with respect to the pure PEMA ($2.23.10^{-17}$ m^3m/m^2sPa) matrix. In the barrier study, the montmorillonite clay shows the best performance with regard to kaolinite, most likely as a result of the higher aspect ratio of the former filler in the compounded resins. It should be kept in mind that permeability measurements have been carried out in hot pressed films where there is not a preferential orientation of

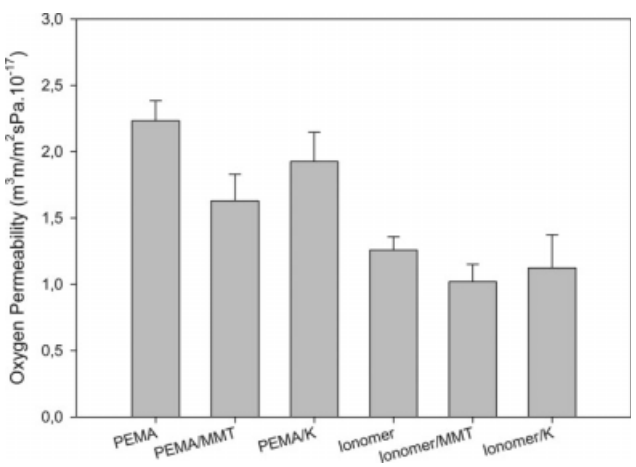

Figure 6 Values of oxygen permeability for neat PEMA, Ionomer and their nanocomposites.

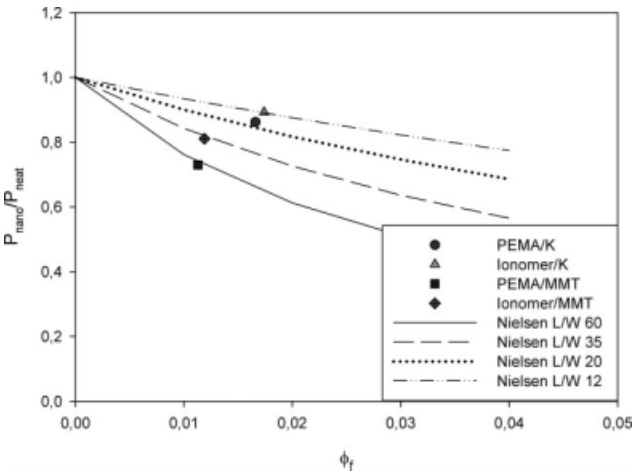

Figure 7 Relative permeability (Pc/Pm) and theoretical curves resulted from application of Nielsen model for several aspect ratios.

the clay layers and the sheet homogeneity is not as good as it can become in industrial extruded films.

The Nielsen permeability model [eq. (4)] is often used to predict the barrier effect of layered particles homogenously dispersed and aligned in the direction perpendicular to the permeant transport.[23,52]

$$\frac{P_c}{P\mathrm{m}} = \frac{1-\phi_f}{1+(L/2W)\phi_f} \tag{4}$$

Where P_c is the permeability of the nanocomposite, P_m is the permeability of the matrix, φ_f is the volume fraction of the filler and L/W is the aspect ratio of the filler.

Figure 7 represents the predicted permeability of nanocomposites versus filler content according to the Nielsen model using several clay particles aspect ratios. The experimental relative permeabilities (P_c/P_m) values fit the Nielsen model for aspect ratios between 12 and 60, being higher for the MMT systems. Therefore, the average aspect ratios predicted with this model are within the rough values estimated from the TEM pictures (Table II) even when the assumptions made by the model may not be exactly met by the two systems. Thus, the higher L/W ratio of montmorillonite particles could explain the lower permeabilities obtained for MMT nanocomposites.

CONCLUSIONS

This study made use of four polymeric matrices (i.e., PEMA, Ionomer, PEAA, and EVA) and of two organoclays (i.e., MMT and K), and studied the dispersion and physical properties of their corresponding nanocomposites prepared using an internal mixer. From the results, the PEMA and ionomer matrices exhibited the best performance in terms of dispersion, mechanical, thermal and barrier properties under the processing conditions applied. Nevertheless, the best level of nanoclay exfoliation for the two organoclays was achieved in the maleated polyethylene matrix (PEMA). Higher aspect ratio was seen for the montmorillonite nanocomposites, in good agreement with the higher improvements in thermooxidative degradation temperatures and oxygen barrier measurements. However, organokaolinite provided better mechanical performance as it could have stronger interfacial interactions with the polymer as predicted by application of the Halpin-Tsai theoretical model. These two matrices, i.e., PEMA and ionomer, could make good compatibilizing systems to disperse organoclays in polyolefin systems.

This work has been financially supported by the Spanish project MEC MAT2006-10261-C03. The authors would like to acknowledge NanoBioMatters S.L. for supplying the clays, to SCIC of Universitat Jaume I for their help in part of the characterization and specially to María Dolores Sánchez-Garcia, Raquel Oliver, and José Ortega for experimental support. M.P. Villanueva expresses her gratitude to Generalitat Valenciana for the doctoral grant CTBPRB/2005/277.

References

1. Osman, M. A.; Rupp, J. E. P.; Suter, U. W. J Mater Chem 2005, 15, 1298.
2. Hadal, R. S.; Misra, R. D. K. Mater Sci Eng A-Structural Mater Properties Microstructure Process 2004, 374, 374.
3. Kwon, S.; Kim, K. J.; Kim, H.; Kundu, P. P.; Kim, T. J.; Lee, Y. K.; Lee, B. H.; Choe, S. Polymer 2002, 43, 6901.
4. Tsuwi, J. K.; Merenga, A. S.; Katana, G.; Papadakis, C. M. J Polym Mater 2003, 20, 355.
5. Fendler, A.; Villanueva, M. P.; Gimenez, E.; Lagaron, J. M. Cellulose 2007, 14, 427.
6. Mishra, A. K.; Luyt, A. S. Polym Degrad Stab 2008, 93, 1.
7. Rizvi, G. M.; Serneralul, H. J Vinyl Additive Technol 2008, 14, 39.
8. Giannelis, E. P. Appl Organomet Chem 1998, 12, 675.
9. Alexandre, M.; Dubois, P. Mater Sci Eng R-Reports 2000, 28, 1.
10. Zhang, M. Q.; Sundararaj, U. Macromol Mater Eng 2006, 291, 697.
11. Zhang, J. G.; Wilkie, C. A. Polym Degrad Stab 2003, 80, 163.
12. Liang, G. D.; Xu, J. T.; Bao, S. P.; Xu, W. B. J Appl Polym Sci 2004, 91, 3974.
13. Kato, M.; Okamoto, H.; Hasegawa, N.; Tsukigase, A.; Usuki, A. Polym Eng Sci 2003, 43, 1312.
14. Hotta, S.; Paul, D. R. Polymer 2004, 45, 7639.
15. Chrissopoulou, K.; Altintzi, I.; Anastasiadis, S. H.; Giannelis, E. P.; Pitsikalis, M.; Hadjichristidis, N.; Theophilou, N. Polymer 2005, 46, 12440.
16. Ranade, A.; Nayak, K.; Fairbrother, D.; D'Souza, N. A. Polymer 2005, 46, 7323.
17. Truss, R. W.; Yeow, T. K. J Appl Polym Sci 2006, 100, 3044.
18. Gopakumar, T. G.; Lee, J. A.; Kontopoulou, M.; Parent, J. S. Polymer 2002, 43, 5483.
19. Preston, C. M. L.; Amarasinghe, G.; Hopewell, J. L.; Shanks, R. A.; Mathys, Z. Polym Degrad Stab 2004, 84, 533.
20. Cabedo, L.; Feijoo, J. L.; Villanueva, M. P.; Lagaron, J. M.; Gimenez, E. Macromol Symp 2006, 233, 191.
21. Cabeda, L.; Gimenez, E.; Lagaron, J. M.; Gavara, R.; Saura, J. J. Polymer 2004, 45, 5233.

22. Itagaki, T.; Matsumura, A.; Kato, M.; Usuki, A.; Kuroda, K. J Mater Sci Lett 2001, 20, 1483.
23. Sanchez-Garcia, M. D.; Gimenez, E.; Lagaron, J. M. J Appl Polym Sci 2008, 108, 2787.
24. Li, Z. J.; Zhang, X. R.; Xu, Z. Mater Technol 2007, 22, 205.
25. Gardolinski, J. E.; Carrera, L. C. M.; Cantao, M. P.; Wypych, F. J Mater Sci 2000, 35, 3113.
26. Frost, R. L.; Kristof, J.; Horvath, E.; Kloprogge, J. T. J Colloid Interface Sci 1999, 214, 109.
27. Frost, R. L.; Kristof, J.; Paroz, G. N.; Kloprogge, J. T. Phys Chem Miner 1999, 26, 257.
28. Frost, R. L.; Kristof, J.; Kloprogge, J. T.; Horvath, E. Langmuir 2001, 17, 4067.
29. Gardolinski, J. E.; Peralta-Zamora, P.; Wypych, F. J Colloid Interface Sci 1999, 211, 137.
30. Gardolinski, J. E.; Ramos, L. P.; de Souza, G. P.; Wypych, F. J Colloid Interface Sci 2000, 221, 284.
31. Komori, Y.; Sugahara, Y.; Kuroda, K. J Mater Res 1998, 13, 930.
32. Komori, Y.; Sugahara, Y.; Kuroda, K. Appl Clay Sci 1999, 15, 241.
33. Komori, Y.; Sugahara, Y.; Kuroda, K. Chem Mater 1999, 11, 3.
34. Tunney, J. J.; Detellier, C. Chem Mater 1993, 5, 747.
35. Tunney, J. J.; Detellier, C. J Mater Chem 1996, 6, 1679.
36. Tunney, J. J.; Detellier, C. Chem Mater 1996, 8, 927.
37. Matsumura, A.; Komori, Y.; Itagaki, T.; Sugahara, Y.; Kuroda, K. Bull Chem Soc Jpn 2001, 74, 1153.
38. Villanueva, M. P.; Cabedo, L.; Lagaron, J. M.; Gimenez, E. 9th European Symposium on Polymer Blends; 2007.
39. Durmus, A.; Woo, M.; Kasgoz, A.; Macosko, C. W.; Tsapatsis, M. Eur Polym J 2007, 43, 3737.
40. Wang, K. H.; Choi, M. H.; Koo, C. M.; Choi, Y. S.; Chung, I. J. Polymer 2001, 42, 9819.
41. Filippi, S.; Marazzato, C.; Magagnini, P.; Minkova, L.; Dintcheva, N. T.; La Mantia, F. P. Macromol Mater Eng 2006, 291, 1208.
42. Wang, K. H.; Koo, C. M.; Chung, I. J. J Appl Polym Sci 2003, 89, 2131.
43. Shah, R. K.; Paul, D. R. Macromolecules 2006, 39, 3327.
44. Durmus, A.; Kasgoz, A.; Macosko, C. W. J Macromol Sci Part B-Physics 2008, 47, 608.
45. Fornes, T. D.; Paul, D. R. Polymer 2003, 44, 4993.
46. Osman, M. A.; Rupp, J. E. P.; Suter, U. W. Polymer 2005, 46, 1653.
47. Zhong, Y.; Janes, D.; Zheng, Y.; Hetzer, M.; De Kee, D. Polym Eng Sci 2007, 47, 1101.
48. Chavarria, F.; Paul, D. R. Polymer 2004, 45, 8501.
49. Available at http://www.galleries.com/minerals/silicate (accessed, 2008).
50. Shah, R. K.; Paul, D. R. Polymer 2006, 47, 4075.
51. Zanetti, M.; Bracco, P.; Costa, L. Polym Degrad Stab 2004, 85, 657.
52. Nielsen, L. E. J Macromol Science, A1 1967, 5, 929.